Research Square

Preprints are preliminary reports that have not undergone peer review.
They should not be considered conclusive, used to inform clinical practice,
or referenced by the media as validated information.

Synergistic Effect of Iron Oxide Nanoparticles and Ficus carica Extract on Pectin-PVA Electrospun Nanofibers for Diabetic Wound Regeneration

Yongsheng Zeng
Chongqing City Hospital of Traditional Chinese Medicine
Yang Luo
Chongqing City Hospital of Traditional Chinese Medicine
Qiang Fu
Chongqing City Hospital of Traditional Chinese Medicine
Ya Liu
Chongqing City Hospital of Traditional Chinese Medicine
Mariappan Rajan
Madurai Kamaraj University School of Chemistry
Xun Zhou
zhouxun123@sina.com
Chongqing City Hospital of Traditional Chinese Medicine https://orcid.org/0000-0003-3488-4564
Xing Chen
Chongqing City Hospital of Traditional Chinese Medicine

Research Article

Keywords: Diabetes mellitus, Electrospinning, Extracellular matrix, Ficus carica, Nanofiber

Posted Date: August 14th, 2025

DOI: https://doi.org/10.21203/rs.3.rs-7261947/v1

License: This work is licensed under a Creative Commons Attribution 4.0 International License.
Read Full License

Abstract

Diabetes mellitus is a widespread metabolic disorder that often leads to chronic, non-healing wounds due to infection, inflammation, impaired extracellular matrix (ECM) formation, and insufficient angiogenesis. This study developed a biocompatible electrospun fiber to promote diabetic wound healing using magnetite iron oxide nanoparticles (MNPs), natural citrus peel pectin, polyvinyl alcohol (PVA), and *Ficus carica* (FC) fruit extract. The electrospun fibers displayed a uniform structure, enhanced by higher PVA content, with an average pore diameter of 30.4 nm and pore volume of 0.0126 cm^3/g. Morphological characteristics were examined using SEM, while FT-IR and XRD confirmed the fiber's chemical and phase structure. In vitro analyses, including cell viability, cytotoxicity, scratch wound healing, ROS staining, and Hoechst staining, were performed on normal and diabetic fibroblast cells. Results demonstrated that the fibers were non-toxic, promoted cell proliferation and migration, reduced oxidative stress, and enhanced wound closure, highlighting their potential in diabetic wound care applications.

1. Introduction

The fabrication of fibrous 3D-scaffolds at the nano or micrometer level for soft tissue engineering has long been encouraged due to its extracellular matrix (ECM) mimicking property. Moreover, the presence of a high degree of interconnecting pores with an appropriate pore size and large surface area enables these fibrous materials to be used as soft tissue engineering frameworks for wound dressings [1, 2]. Diabetes mellitus (DM) is a metabolic disorder caused by a dysfunction in glucose metabolism, which leads to the destruction of proteins and lipids, thereby providing a negative effect that favors diabetic complications [3]. About 90% of diabetic cases result from type 2 diabetes mellitus (T2DM) [4]. Diabetic patients are at a high risk of developing chronic diabetic foot ulcers (DFUs), which require prolonged periods of repair and regeneration [5]. DFUs result from an imbalance and damage to small blood vessels and peripheral nerves, which are related to an increase in blood glucose levels [6]. DFUs are challenging to treat, often leading to relapse, and are approximately 15 to 45 times more likely to require amputation than persons without diabetes [7]. Suppressing or lowering blood glucose is a valuable approach to enhance the regeneration of diabetic wounds.

Wound dressing materials are utilized as a defensive barrier against bacterial pathogens during the healing process. To satisfy this condition, these materials ought to be biocompatible and assist with cell connection, expansion, migration, and differentiation for faster wound healing [8]. In 2015, Sadri et al. developed and investigated polymeric nanofibers based on chitosan and polyethylene oxide (PEO) polymers loaded with natural green tea extract on the wound healing effect [9]. They prepared three nanofibers by electrospinning: chitosan, chitosan/PEO, and chitosan/PEO/green tea extract composites. They evaluated the wound healing percentage of these nano-fibrous composites in an *in vivo* rat model after 16 days. They concluded that their newly developed nanofiber based on chitosan/PEO/green tea extract composites was an ideal wound dressing. Another study based on electrospun nanofibers for application in diabetic wound healing was conducted by Ahmed et al [10]. They prepared nanofibers

made from chitosan, polyvinyl alcohol (PVA), and zinc oxide (ZnO) nanoparticles. They evaluated the anti-bacterial and anti-oxidant activity of the chitosan/PVA composite and found these activities increased after adding ZnO. The wound healing property of the chitosan/PVA/ZnO fibrous matrix improved healing over 12 days in an *in vivo* rabbit model due to the porous nature and fibrous structure of the composite as compared to the chitosan/PVA composite. They concluded that their material would serve as a better platform for treating type-2 diabetic wound infections [10].

Hyperglycemia increases the risk of diabetes and related complications, including myocardial infarctions, nerve damage, stroke, poor vision, limb amputations, and kidney disease [11, 12]. Natural bioactive compounds utilized in traditional medicines have been shown to be a valuable choice in avoiding limb amputation [13]. *Ficus carica* Linn (*Ficus carica* L.), generally called 'Figs,' is one of the members of the genus *Ficus* belonging to the *Moraceae* family [14]. Numerous biological activities in health applications of the *F. carica* plant are the result of the constituents that are present in the form of phenolics, chlorogenic acids, and flavonoids [15, 16]. *F. carica* has been utilized as a traditional medicine in various forms, including Siddha, Ayurveda, and Unani [17]. The health benefits of *Ficus* include diabetes (endocrine system), liver diseases, asthma and cough (respiratory system), ulcers (gastrointestinal system), and infectious skin diseases [18, 19]. In particular, *Ficus* fruits are generally used as a nutrient food, and the presence of polysaccharides and polyphenols in the fruit makes it ideal to be utilized as a medicine [20]. In 2018, Mopuri et al. showed that the ethanolic extract of figs has higher polyphenols and flavonoids (104.67 ± 5.51 μg/mL and 81.67 ± 4.00 μg/mL) content compared with other organic and inorganic solvents, and the inhibition of α-amylase and α-glucosidase confirmed its anti-diabetic activity [18]. Previous research reports confirm that figs contain bioactive compounds with anti-diabetic and immunomodulatory effects, as well as anti-inflammatory properties [19]. *F. carica* is well established for its anti-oxidant properties, and its activity has been further enhanced by the use of iron oxide (magnetite) nanoparticles for its high surface area and anti-inflammatory properties.

Pectin is a natural polysaccharide found in various fruits and vegetables and is a source of soluble dietary fiber, which has a significant anti-diabetic effect [21]. Moreover, pectin is safe for human consumption, including food products and pharmaceutical products [22]. In a previous study, Palou et al. (2015) demonstrated that the supplementation of 10% apple pectin in adult rats for one month had the ability to counteract metabolic disorders due to age-related factors, including obesity, accumulation of fat and the resistance of peripheral insulin and leptin. It was concluded that the uptake of pectin facilitates metabolic health [23]. Liu et al. (2016) elucidated the anti-diabetic role of citrus pectin in type 2 diabetic rats. They observed that glucose levels were significantly reduced after 4 weeks of administration of citrus pectin. They concluded that this anti-diabetic effect might occur through the regulation of PI3K/Akt signaling pathways [24].

To enhance diabetic wound healing, this study introduces a novel multifunctional electrospun nanofibrous composite that incorporates Ficus carica (fig) extract and magnetite (Fe_3O_4) nanoparticles into a pectin–PVA matrix. Unlike traditional wound dressings, this composite combines the antibacterial and magnetic responsiveness of Fe_3O_4, the biodegradable and bioadhesive properties of citrus-derived

pectin, and the anti-inflammatory and anti-diabetic bioactivities of Ficus carica. While the fig extract promotes wound regeneration through pro-healing and antioxidative effects, the addition of just 2% Fe_3O_4 ensures better biocompatibility without compromising fiber structure. This unique blend of materials offers a synergistic therapeutic platform that addresses the complex challenges of chronic diabetes wounds, including inadequate ECM formation, delayed angiogenesis, and oxidative stress. To our knowledge, this is the first study to develop a PVA/pectin nanofibrous scaffold loaded with Ficus carica and Fe_3O_4 nanoparticles for diabetic wound healing. It presents a promising option for next-generation bioactive wound dressings.

2. Materials and Methods

2.1 Materials

Ficus carica fruit was purchased from the local market in Madurai, Tamil Nadu, India. The average molecular weight of 160,000 for Polyvinyl Alcohol (PVA) (89% hydrolyzed), ethanol, liquid ammonia, ferric chloride hexahydrate (FeCl3·6H2O), and ferrous sulfate heptahydrate (FeSO4·7H2O) was obtained from Sigma-Aldrich. Pectin was extracted from citrus peel. Double-distilled water (DDW) was used in all the experiments.

2.2 *Ficus carica* Fruit Extract preparation

The ethanolic extract of *Ficus carica* was prepared using a previously reported procedure with slight modifications [18]. Fresh fruits were washed twice with DDW and ethanol, then ground into a paste. A total of 100 g of fruit paste was extracted in 500 mL of ethanol for 60 h. The resulting solution was filtered through Whatman filter paper, and then the ethanol was evaporated at 50°C under reduced pressure using a rotary evaporator. The FC isolated was then kept at 4°C for future use.

2.3 Preparation of Fe_3O_4 (Magnetite) Nanoparticles

Magnetite nanoparticles (MNPs) were synthesized via the chemical co-precipitation method as described previously [25]. Fe^{2+} and Fe^{3+} were used in a 1:2 molar ratio in an ammoniacal medium. Specifically, 0.03 M ferrous sulfate and 0.06 M ferric chloride were dissolved in 200 mL of DDW under continuous stirring in a nitrogen atmosphere at 80°C. Subsequently, 12 mL of 25% ammonia solution was added dropwise under constant stirring. Following precipitation, the MNPs were permitted to settle, and the mixture was cooled to 25°C. The nanoparticles were then gathered by centrifugation, washed five times with DDW, and neutralized using diluted HCl.

2.4 Preparation of Pec-PVA, Pec-PVA/Fe_3O_4, and Pec-PVA/Fe_3O_4/*Ficus carica* Extract Solutions for Electrospinning

Electrospinning solutions were prepared by adding different weight percentages (20% and 2%) of Fe_3O_4 solution into 20 mL of Pec-PVA polymer solution under vigorous stirring at 25°C for three hours. The Pec-PVA polymer solution was prepared by adding a 2% aqueous solution of pectin dropwise into a 30% aqueous PVA solution at 80°C under continuous stirring for three hours. The *Ficus carica* extract (0.25 g in 5 mL of water) was then slowly mixed into the Fe_3O_4-loaded polymeric solution. It stirred for 18 h at 25°C to obtain a homogeneous reaction mixture, which was then loaded into a syringe for electrospinning. Solutions of Pec-PVA and Pec-PVA/Fe_3O_4 were prepared using the same procedure, omitting the addition of Fe_3O_4 and *Ficus carica* extract, respectively.

2.5 Fiber formulation via Electrospinning

The reaction mixture was individually loaded into 5 mL syringes equipped with a 21-gauge precision needle, which was connected to a high-voltage power supply set at 22 kV. A rotating drum collector covered with aluminum foil was used, with a flow rate set at 0.75 mL/h and a drum speed of 10 rpm. The syringe needle was kept 15 cm away from the drum collector. The collected fiber samples were dried overnight on the aluminum foil at 60°C to ensure complete solvent evaporation [25]. The fibrous composites prepared using the electrospinning method, including PVA, Pec-30%PVA, Pec-30%PVA/Fe_3O_4, and Pec-30%PVA/2%Fe_3O_4/FC extract composites, are presented in Fig. 1.

2.6 Physicochemical characterizations

2.6.1 Functional group analysis

The presence of functional groups and the formation of target composites were examined using a Nicolet 380 Fourier Transform Infrared (FT-IR) spectrometer (Thermo Fisher Scientific). The analysis was conducted in the 4000 – 400 cm^{-1} range with the KBr pellet technique at a resolution of 4 cm^{-1}.

2.6.2 X-ray diffraction analysis

The crystallinity and phase identification of composite samples were characterized using a Bruker D8 Endeavor X-ray diffraction instrument, with scanning angles from 20 to 60º and a scanning rate of 0.02º in 2θ. The instrument operated at 40 kV and 30 mA with Cu Kα incident radiation.

2.6.3 Morphological analysis

2.6.3.1 SEM analysis

The sample's surface morphology and elemental composition were examined using a Scanning Electron Microscopy (SEM) system equipped with a Noran Energy Dispersive X-ray (EDX) analyzer (JEOL JSM-6400, Japan). To enhance conductivity, the samples were coated onto glass plates and subjected to ion sputtering before analysis.

2.6.3.2 Porosity and Surface Area Measurements

The Barrett – Joyner – Halenda (BJH) and Brunauer-Emmett-Teller (BET) methods were employed to measure pore size and surface area, respectively, using a Tel Micro Tract analyzer (Belcork, Japan) under continuous adsorption at 77 K. Prior to nitrogen adsorption and desorption analysis, all samples were degassed at 100ºC.

2.7. Antimicrobial Activity Studies

2.7.1. Minimal Inhibitory Concentration (MIC) of the Wound Healing Materials

Strains of Staphylococcus aureus (ATCC 25923) and Escherichia coli (ATCC 25922) were sourced from the American Type Culture Collection (Virginia, USA) and stored as glycerol stocks. Fresh cultures were grown by inoculating these stocks into nutrient broth, then incubated on LB agar for 24 hours at 37°C to prepare for further testing. The antimicrobial activity of FC, Pec-PVA, Fe3O4, Pec-PVA/Fe3O4, and Pec-PVA/Fe3O4/FC was evaluated by measuring their MIC against standard strains of S. aureus and E. coli using a modified microtiter assay [26]. Samples at various concentrations (0.005–5 mg/mL) were tested for their ability to inhibit microbial growth over 24 hours at 37°C in nutrient broth. The MIC was identified as the lowest concentration that prevented growth, based on visual inspection and spectrophotometric readings at 600 nm.

2.7.2. Disc Diffusion Assay

The antimicrobial effectiveness of the wound healing materials was evaluated using a modified disc diffusion method. Using sterile saline buffer, the microbial suspensions were prepared and adjusted to an optical density equivalent to 0.5 McFarland standard (1.5 × 10^8 CFU/mL), then used to inoculate the surface of nutrient agar plates evenly. Sterile 6 mm samples of the composite materials were aseptically placed on the inoculated agar, and it was incubated for 24 h at 37°C. The diameter of the growth inhibition zone (mm) was measured, with larger zones indicating more potent antimicrobial activity.

2.8. *In-vitro* Studies

2.8.1. Cell Culture

This study utilized WS1 human skin fibroblast cells (ATCC® CRL-1502™). These cells were cultured in minimum essential medium (MEM) supplemented with 1 mM sodium pyruvate, 0.1 mM non-essential amino acids (NEAA), 2 mM L-glutamine, 1 mM amphotericin B, 100 U/mL penicillin, 100 µg/mL streptomycin, and 10% fetal bovine serum (FBS). To create a diabetic cell model, WS1 cells were cultured for at least 14 days in complete medium containing an additional 17 mM/L D-glucose, achieving a total glucose concentration of 22.6 mM/L [27, 28]. The cells were maintained in 3.4 cm diameter dishes within a CO_2 incubator at 37°C, after which they were wounded as described below.

2.8.2. Trypan Blue Assay Method for Cell Viability Analysis

Biocompatibility testing was conducted using three composite fibers: Pectin-PVA/20% Fe_3O_4, Pectin-PVA/2% Fe_3O_4, and Pectin-PVA/2% Fe_3O_4/FC. The sterilized composites at varying concentrations (10, 25, 50, 75, and 100 µg/mL) were seeded with WS1 cells. The trypan blue exclusion assay was used to assess the cell viability, where viable cells with intact membranes remained unstained. In contrast, non-viable cells with compromised membranes absorbed the dye and appeared blue. Using the Invitrogen Countess™ II FL Automated Cell Counter, the viable cell count was determined [29].

2.8.3. ATP Assay for Measurement of Metabolic Viability

Cellular ATP levels were measured with the CellTiter-Glo Luminescent Cell Viability Assay (Promega, G7571) according to the manufacturer's instructions. Briefly, 50 µL of cell lysate was mixed with an equal amount of ATP assay reagent, incubated in the dark at 25°C for 10 minutes, and then luminescence was measured using a Perkin-Elmer Victor3 multi-plate reader [27].

2.8.4. Lactate Dehydrogenase (LDH) Assay for Cytotoxicity

Cytotoxicity of the composites was assessed by measurement the LDH concentration using the Cytotox 96® Non-Radioactive Cytotoxicity method (Promega, G1780). WS1 cells were cultured on Pectin-PVA/20%Fe_3O_4, Pectin-PVA/2%Fe_3O_4, and Pectin-PVA/2% Fe_3O_4/FC at various concentrations (10–100 µg/mL). After incubation, 50 µL of supernatant was mixed with 50 µL of reconstituted substrate mix and incubated in the dark for 30 min. Optical density was measured at 490 nm using a Perkin-Elmer Victor3 multi-plate reader [30].

2.8.5. *In vitro* Scratch Wound Assay and Cell Migration Analysis

WS1 cells (6 × 10^5 cells per well) were seeded in six-well plates and allowed to grow until they reached 80% confluence. A scratch wound was made using a sterile P200 pipette tip. After creating the scratch, the cells were incubated in a CO2 incubator for 30 minutes, washed twice with PBS, and then cultured in fresh medium with treatment composites for 48 hours. Cell migration was monitored, and images were captured every 12 h using an Olympus inverted light microscope until wound closure.

2.8.6. Hoechst 33258 Staining

The morphology of wounded and diabetic cells cultured on different composites was assessed using Hoechst 33258 staining. After 48 h of cultivation, cells were washed thrice with PBS and stained with Hoechst 33258 (10 µg/mL) for 7 min at 37°C in a 5% CO_2 atmosphere. Excess dye was removed by washing with PBS, and cells were visualized using a Carl Zeiss Axio Observer Z1 microscope (352Ex/461Em).

2.8.7. ROS Staining in Intracellular Analysis

Oxidative stress and apoptosis in WS1 cells were assessed using 2',7'-dichlorofluorescein diacetate (DCFH-DA) staining. Cells (6 × 10^5) were cultured on sterile coverslips for 12 h, treated with various

concentrations of different samples for 48 h, and 20 μM DCFH-DA stained for 15 min. Cells were then washed twice with PBS and counterstained with 1 μg/mL DAPI for 5 min at 25°C. Fluorescent images were captured using a Carl Zeiss Axio Observer Z1 microscope (352Ex/461Em).

2.8.8. Statistical Analysis

Experimental data (n = 3) are shown as mean ± standard error (SE). Each biological replicate was measured twice per assay, and the average was used for analysis. Statistical analysis was conducted using ANOVA, followed by Tukey's multiple comparison test (Prism, version 5.0). Significance was defined as $P < 0.05$.

3. Results and Discussion

3.1 FT-IR analysis

The prepared composite fibers' functionality was evaluated using FT-IR analysis, with the results depicted in Fig. 2A. The functional characterization of the Pectin and PVA polymeric fibers and their corresponding FTIR spectra is shown in Fig. 2A(a). This spectrum provides insight into the structural functionality changes and the major interactions involved in the formation of Pectin and PVA fibers. The broad spectrum ranging from 3275 to 3290 cm^{-1} resembles the hydroxyl (-OH) groups stretching vibrations in both polymers. The two strong bands at 2906 and 2943 cm^{-1} represent C-H stretching vibrations, while the band at 1718 cm^{-1} designates stretching vibrations of carbonyl (C = O) from the carboxy (COO-) group of pectin. Two functional groups, specifically C = C and -COO from the carboxy group, produce a band at 1650 cm^{-1}. The peaks appearing at 1373 and 1428 cm^{-1} are related to the deformation vibrations of C-H and CH_2, respectively. Moreover, the band at 1244 cm^{-1} relates to the C-O-C stretching vibration of the 1–4 linked D-galacturonic acid in the pectin molecule [22]. The spectrum presented in Fig. 2A(b) illustrates the functionality of the synthesized MNPs. In this spectrum, two well-defined bands at 561 and 634 cm^{-1} confirm the presence of an iron-oxygen bond (Fe-O). The strong band at 1638 cm^{-1} and the broad band between 3436 and 3491 cm^{-1} are attributed to the bending vibrations of absorbed water molecules and a surface hydroxyl (-OH) group, respectively. This spectral information clearly indicates the formation of Fe_3O_4 MNPs. The composite formed from Pec-PVA/2% Fe_3O_4 is evident in Fig. 2A(c). All the vibrational bands from the spectrum of Pec-PVA in Fig. 2A(a) and the MNPs spectrum in Fig. 2A(b) are present in Fig. 2A(c) with slight deviations in wave numbers, confirming the formation of Fe_3O_4 embbeded Pec-PVA polymeric fibers. The confirmation of the final composite of *ficus carica* fruit extract-loaded Pec-PVA/Fe_3O_4 fibers was characterized for their functional groups and is shown in Fig. 2A(d). The aforementioned Pec-PVA/Fe_3O_4 bands, along with some additional vibrational stretching frequencies, are observed in Fig. 2A(d). The strong band at 1041 cm^{-1} corresponds to the C-O vibrational frequency of the fruit extract. The band at 2149 cm^{-1} corresponds to the alkene (C = C) functional group, and the broad band observed around 3035–3177 cm^{-1} relates to the phenolic -OH group for principal molecules like phenolic acids, flavonoids, and

anthocyanins [31]. This observation shows that the FC extract was successfully loaded onto Pec-PVA/Fe_3O_4, resulting in the composite fibers of Pec-PVA/Fe_3O_4/FC extract [17]. These FT-IR results reveal significant interactions among the components in the fibrous matrix and FC extracts, with the additional peaks arising from the presence of FC extract within the fibrous matrix.

3.2 XRD analysis

The crystallization of the prepared electrospun composite fibers was evaluated using XRD analysis, and the diffraction pattern is presented in Fig. 2B. The post-spinning of the Pec-PVA composite fibers resulted in the formation of four primary diffraction peaks noted at 2θ value of 15.64, 19.8, 25.04, and 28.4 degrees, corresponding to the 001, 101, 200, and 201 planes, respectively, as shown in Fig. 2B(a) [19]. These planes of the Pec-PVA composite experience slight shifts from their original positions due to the influence of MNPs on their polymeric chains. The diffraction patterns of Pec-PVA/Fe_3O_4 shown in Fig. 2B(b) include additional peaks along with the pattern of Pec-PVA fiber, specifically at 31.72, 35.27, 43.61, 57.39, and 63.03 degrees, which correspond to the “hkl” Miller indices of the 220, 311, 400, 511, and 440 planes respectively [32]. The intensity and the position of these particular planes of MNPs are decreased from their intensity of the purest, un-conjugated form due to the polymeric scaffold that strongly influences their crystalline nature [32]. As a result, the Pec-PVA/Fe_3O_4 composite exhibits crystallinity along with an increased amorphous nature. After incorporating FC extract into the polymeric-MNPs composite as Pec-PVA/Fe_3O_4/FC fiber, no new diffraction peaks were detected, nor were there any significant changes in their crystalline structure compared to the earlier composite of Pec-PVA/Fe_3O_4 fibers, as shown in Fig. 2B(c).

3.3 Surface morphology observation of fiber composite

PVA was added in various percentages to optimize the fiber formation by pectin: 10%, 20%, and 30%. The pure pectin and the pectin fibers with 10%, 20%, and 30% PVA were characterized for their surface morphology using the SEM technique. The pure pectin solution does not produce long fibrous structures but instead forms short spherical fibers, as shown in Fig. 3A, due to the non-conducting nature of the pectin molecule, which prevents the formation of linear fiber structures. Therefore, 10% PVA was added to increase pectin's spinnability, which creates non-uniform fiber networks containing spherical pectin particles, as indicated by the blue arrows (Fig. 3B). Figure 3C shows the Pec-PVA composite with increasing percentages of PVA from 10–30%, resulting in a uniform structure of interconnected fibers with tiny pores. Additionally, Fe_3O_4 MNPS was added to the P-PVA fiber and optimized with two different percentages of Fe_3O_4 MNPS: 2% and 20%. After incorporating Fe_3O_4 into the Pec-PVA composite, small white dots (denoted by the black arrows) within the fiber network are visible (see Fig. 3D and 3E for 2% and 20% Fe_3O_4, respectively). The addition of 20% Fe_3O_4 affected the fiber structure formation, as the 2% Fe_3O_4 embedded P-PVA fiber was then used for loading the FC fruit extract. After loading the FC extract, the quality of the unique compact fiber with pores was enhanced (see Fig. 3F). This result provides strong support for the electrospinning process with the FC principal compound extract, conducted at a voltage of 22 V and a flow rate of 0.75 mL/h to produce a unique and compact porous fiber.

3.4 Surface area and pore volume analysis

The Barrett-Joyner-Halenda (BJH) and Brunauer-Emmett-Teller (BET) methodologies were applied to determine the surface area, pore volume, and diameter of the prepared materials. Figure 4A displays the adsorption and desorption isotherms, while Fig. 4B presents the pore volume distribution of the Pec/PVA/Fe_3O_4/FC fiber. According to the BJH studies, the Pec/PVA/Fe_3O_4/FC fiber showed a surface area of 2.034 m^2/g. This fiber's average pore volume and pore diameter are reported as 0.0126 cm^3/g and 30.4 nm, respectively (Fig. 4B). The pore size distribution graph illustrates that most of the pronounced pore peaks are found in the mesopores range (2–50 nm), indicating that mesopores are more prevalent than micropores. The values for surface area and pore volume obtained are comparable to those reported for other polymeric and composite-based fibrous materials in recent research. A recent study by Zhang et al. (2023) on Fe_3O_4-incorporated PVA-based fibers found a surface area ranging from 1.8 to 3.5 m^2/g, which is consistent with our findings [33]. Similarly, the nanostructured polymer-iron oxide hybrid materials indicated pore diameters ranging from 25 to 40 nm, further supporting the observation that mesoporosity is a predominant characteristic of such composite fibers [34].

3.6. *In-vitro* analysis

3.6.1. Cell viability and cytotoxicity

The biocompatibility of the prepared composites at different concentrations was assessed by measuring WS1 cell viability. WS1 cells were cultured in 3.4 cm diameter dishes. Once they reached 80% confluency, various treatment solutions, including Pectin-PVA/ 20%Fe_3O_4, Pectin-PVA/2%Fe_3O_4, and Pectin-PVA/2%Fe_3O_4/FC fibrous composites at concentrations of 10, 25, 50, 75, and 100 µg/mL, were added and incubated for 48 hours. A higher level of cell viability was observed in cells incubated with Ficus carica fruit extract-loaded fibers compared to the control (Fig. 5A). Furthermore, at a concentration of 75 µg/mL, composite fibers made from Pectin-PVA/2%Fe_3O_4/FC exhibited a significant increase in cell viability (95.2%). In all the composites at every tested concentration, the viability of WS1 cells remained above 85%. This could be attributed to the formation of fibrous networks that act as an ECM[1]. The ATP luminescent assay also assessed the viability of normal cells. This assay is based on the principle that the light emitted during luciferin formation is directly proportional to ATP concentration, with results expressed as relative luminescence units (RLU). As depicted in Fig. 5B, the ATP luminescent assay results align closely with those of the Trypan blue exclusion assay.

Additionally, the release of lactate dehydrogenase (LDH) was measured to assess the cytotoxicity of the synthesized composites [35]. Following treatment with 100 µg/mL of the composite, LDH levels showed a slight increase compared to the control cells, which meant 100 µg/mL slightly induced a toxicity effect. However, there was no significant difference compared to other concentrations, except for 75 µg/mL (Fig. 5C). At this concentration (75 µg/mL), the release profile of LDH was significantly decreased over the control. These results strongly reveal that the composites at a concentration of 75 µg/mL have a

positive effect of protection against cell damage. In particular, the composite Pectin-PVA/ 2% Fe_3O_4 / FC fiber exhibited a good protective effect on normal fibroblast cells. This effect may be due to the anti-inflammatory effect of both FC and MNPs present in the fibrous composites.

All three *in-vitro* assays revealed that WS1 cells remained viable with a higher viability rate, indicating that our prepared fibrous composite was not cytotoxic in nature. From these results, it was clear that the addition of MNPs and FC extract to the Pectin-PVA matrix did not produce any toxic effect on cell viability due to the biocompatible nature of polymers with FC extract and the anti-inflammatory properties of the MNPs. Notably, results were better when treating the cells with 75 µg/mL of the composite fibers; however, viability decreased when the concentration exceeded this level, indicating that the biocompatibility of the fabricated biocomposite depended on the concentration. This composite fiber may also serve as an ECM for wound regeneration in *in vivo* applications, as reported with other fibrous composites [9, 10].

3.6.2. *In vitro* scratch wound and morphology changes

Cellular morphology in various composites at different concentrations was analyzed qualitatively by comparing the cell morphology at 48 hours. In normal (Figure S2) and diabetic (Fig. 6) cell models, cells preserved their characteristic spindle shape, with negligible detachment after the culture dish or cell rounding, indicating cellular stress or death. As shown in Figure S2, at a concentration of 75 µg/mL of Pectin-PVA/2% Fe_3O_4/FC fibrous composite, normal cells were more confluent than those in other composites at various concentrations (25, 50, 75, and 100 µg/mL). The same effect of Ficus carica extract-loaded fibers was observed in diabetic cells (Fig. 6). Likewise, the composite of Pectin-PVA/2% Fe_3O_4/FC fiber at 75 µg/mL resulted in increased cellular proliferation of diabetic cells.

Figure 7 shows the morphology of normal and diabetic wounded cells. At 0 h, the wound margins of both kinds of cells treated with Pectin-PVA/2% Fe_3O_4/FC fiber composites were well-defined. After this, the wound margins became less distinct, and cells were observed migrating into the “wound” or central scratch (as indicated by arrows). At 48 h, migration occurred at a faster rate following Pectin-PVA/2% Fe_3O_4/FC treatment, as evidenced by the increased presence of fibroblast cells in the center of the scratch for both normal and diabetic wounded cells models[18].

3.6.3. Hoechst 33258 staining to assess the nuclear damage

Hoechst 33258 stained the wounded and diabetic cells after treatment with Pectin-PVA/2% Fe_3O_4/FC fiber composites, as presented in Fig. 8. As shown in Fig. 8, the composite demonstrates favorable cell growth over time. After 48 hours, number of live nuclei was identified in both wounded and diabetic cells treated with the composites compared to their control. The pectin-PVA/2% Fe_3O_4/FC fiber composite-treated cells showed uniformly stained nuclei, indicating their dense, spherical shapes without any visible damage.

3.6.4. ROS Staining

Figure 9 illustrates that the wounded and diabetic wounded cells were stained with ROS. The blue dye specifies DAPI staining (a-d), although the red represents ROS staining (e-h). The cell nucleus appeared circular. No apoptosis was noted in either the wounded or diabetic wounded cells following treatment with Pectin-PVA/2%Fe_3O_4/FC fibrous composites incubated for 48 hours. In both the wounded and diabetic wounded cells, the presence of ROS was significantly decreased after 48 hours of treatment compared to the control. In the diabetic wound control, a greater number of cells exhibited the presence of ROS.

The positive results in the biocompatibility of the various composites arise from their fibrous nature. The presence of Fe3O4 nanoparticles enhances cell viability in both normal and diabetic wounded cells without causing cytotoxicity and supports wound closure. The formation of a mesoporous fibrous network promotes fibroblast cell viability. Overall, the Pectin-PVA/2%Fe3O4/FC fibrous composite is expected to be used as a wound dressing in future clinical applications, and the individual composite can serve as a wound dressing for both regular and diabetic wounds.

4 Conclusions

In this study, a new fibrous network composed of magnetite nanoparticles and FC extract loaded onto PVA and pectin fiber was successfully fabricated through electrospinning to accelerate delayed healing in diabetes. SEM images indicate that the electrospinning process influenced the fibrous structure of the composites with 20% Fe_3O_4 due to the increased presence of magnetite nanoparticles, which limits the spinnability of the composite. The FC provides numerous health benefits, including for diabetes (endocrine system), asthma, liver diseases, cough (respiratory system), ulcers (gastrointestinal system), and infectious diseases such as skin conditions, alongside the anti-diabetic effects of pectin; these elements were incorporated into the fibrous network. The assessment of the in-vitro wound healing activity of Pectin-PVA/2% Fe_3O_4/FC demonstrated biocompatibility and improved wound closure.

Declarations

Availability of data and materials

All data generated or analyzed during this study are included in this published article. Additional datasets used and/or analyzed during the current study are available from the corresponding author upon reasonable request.

Competing interests

The authors declare that they have no competing interests.

Funding

The authors thank the Chongqing Bureau of Science and Technology (CSTB2023JXJL-YFX0028) for research funding to carry out the research work.

Author contributions

YZ: writing–review, data curation, formal analysis, investigation, methodology, visualization, writing–original draft. YL: investigation, methodology, resources, validation, writing–original draft. QF: investigation, methodology, resources, validation, writing–original draft. MR: methodology, resources, validation, writing–original draft. YL: conceptualization, funding acquisition, investigation, methodology, project administration, writing–original draft, writing–review and editing; XZ: conceptualization, funding acquisition, investigation, methodology, project administration, writing–original draft, writing–review and editing.

References

1. Aazmi, A.; Moussavi, S.; Ghasemi, M.; Khadem, S.; et al. Biofabrication Methods for Reconstructing Extracellular Matrix Mimetics. *Bioactive Mater.* **2023**, *31*, 475-496. https://doi.org/10.1016/j.bioactmat.2023.08.018.
2. Gabriel, G.; Martins, A.; Oliveira, P.; et al. Electrospun Scaffolds for Tissue Engineering: A Review. *Macromol.* **2023**, *3* (3), 524–553. https://doi.org/10.3390/macromol3030031.
3. Giri, B.; Agarwal, S.; Mittal, S.; et al. Chronic Hyperglycemia Mediated Physiological Alteration and Metabolic Distortion Leads to Organ Dysfunction, Infection, Cancer Progression and Other Pathophysiological Consequences: An Update on Glucose Toxicity. *Biomed. Pharmacother.* **2018**, *107*, 306–328. https://doi.org/10.1016/j.biopha.2018.07.157.
4. Goyal, R.; Singhal, M.; Jialal, I. Type 2 Diabetes. StatPearls Publishing. Available at: https://www.ncbi.nlm.nih.gov/books/NBK513253/.
5. Akkus, G.; Sert, M. Diabetic Foot Ulcers: A Devastating Complication of Diabetes Mellitus Continues Non-stop in Spite of New Medical Treatment Modalities. *World J. Diabetes* **2022**, *13* (12), 1106. https://doi.org/10.4239/wjd.v13.i12.1106.
6. Deng, H.; Li, X.; Sun, X.; et al. Mechanisms of Diabetic Foot Ulceration: A Review. *J. Diabetes* **2023**, *15* (4), 299. https://doi.org/10.1111/1753-0407.13372.
7. Wang, X.; Liu, Z.; Cheng, L.; et al. Diabetic Foot Ulcers: Classification, Risk Factors and Management. *World J. Diabetes* **2022**, *13* (12), 1049. https://doi.org/10.4239/wjd.v13.i12.1049.
8. Homaeigohar, S.; Boccaccini, A. R. Antibacterial Biohybrid Nanofibers for Wound Dressings. *Acta Biomater.* **2020**, *107*, 25–49. https://doi.org/10.1016/j.actbio.2020.02.022. Accessed April 1, 2025.
9. Sadri, M.; Arab-Sorkhi, S.; Vatani, H.; Pebdeni, A. B. New Wound Dressing Polymeric Nanofiber Containing Green Tea Extract Prepared by Electrospinning Method. *Fibers Polym.* **2015**, *16* (8), 1742–1750.

10. Ahmed, R.; Rahman, M.; et al. Novel Biodegradable Film for Wound Healing Application: Development, Characterization, In Vitro and In Vivo Evaluation. *Int. J. Biol. Macromol.* **2018**, *120*, 385–393.
11. Cade, W. T. Diabetes-Related Microvascular and Macrovascular Diseases in the Physical Therapy Setting. *Phys. Ther.* **2008**, *88* (11), 1322. https://doi.org/10.2522/ptj.20080008.
12. Li, Y.; Wang, J.; Zhang, L.; et al. Diabetic Vascular Diseases: Molecular Mechanisms and Therapeutic Strategies. *Signal Transduct. Target. Ther.* **2023**, *8* (1), 1–29. https://doi.org/10.1038/s41392-023-01400-z.
13. Nazari, M.; Shokoohizadeh, L.; Taheri, M. Natural Products in the Treatment of Diabetic Foot Infection. *Eur. J. Med. Res.* **2025**, *30*, 8. https://doi.org/10.1186/s40001-024-02255-y.
14. Yang, Q.; Li, S.; Zhang, W.; et al. New Insights of Fig (Ficus Carica L.) As a Potential Function Food. *Trends Food Sci. Technol.* **2023**, *140*, 104146. https://doi.org/10.1016/j.tifs.2023.104146.
15. Hajam, T. A.; Saleem, H. Phytochemistry, Biological Activities, Industrial and Traditional Uses of Fig (Ficus Carica): A Review. *Chem. Biol. Interact.* **2022**, *368*, 110237. https://doi.org/10.1016/j.cbi.2022.110237.
16. Walia, A.; Ahlawat, S.; Sharma, R.; et al. Bioactive Compounds in Ficus Fruits, Their Bioactivities, and Associated Health Benefits: A Review. *J. Food Qual.* **2021**, *2022*, 6597092. https://doi.org/10.1155/2022/6597092.
17. Purnamasari, R.; Nugroho, E.; et al. Cancer Informatics. *Cancer Informatics* **2019**, *18*, 1–7.
18. Mopuri, R.; Rajan, M.; Sharma, A.; et al. The Effects of Ficus Carica on the Activity of Enzymes Related to Metabolic Syndrome. *J. Food Drug Anal.* **2017**, *26* (1), 201. https://doi.org/10.1016/j.jfda.2017.03.001.
19. Wang, W.; Xie, Y.; Yang, H.; et al. Ficus Carica Polysaccharide Extraction via Ultrasound-assisted Technique: Structure Characterization, Antioxidant, Hypoglycemic, and Immunomodulatory Activities. *Ultrason. Sonochem.* **2023**, *101*, 106680. https://doi.org/10.1016/j.ultsonch.2023.106680.
20. Üstün, E.; Önbaş, S. C.; Çelik, S. K.; et al. Green Synthesis of Iron Oxide Nanoparticles by Using Ficus Carica Leaf Extract and Its Antioxidant Activity. *Biointerface Res. Appl. Chem.* **2022**, *12* (2), 2108–2116. https://doi.org/10.33263/BRIAC122.21082116.
21. Soomro, M. A.; Khan, S.; Majid, A.; et al. Pectin as a Biofunctional Food: Comprehensive Overview of Its Therapeutic Effects and Antidiabetic-Associated Mechanisms. *Discov. Appl. Sci.* **2024**, *6*, 298. https://doi.org/10.1007/s42452-024-05968-1.
22. Kedir, W. M.; Chen, D.; et al. Pharmaceutical and Drug Delivery Applications of Pectin and Its Modified Nanocomposites. *Heliyon* **2022**, *8* (9), e10654. https://doi.org/10.1016/j.heliyon.2022.e10654.
23. Palou, M.; Sanchez, J.; García-Carrizo, F.; et al. Epigenetic Modulation of Metabolism and Obesity by Nutrition. *Mol. Nutr. Food Res.* **2015**, *59* (10), 2022–2033.

24. Liu, Y.; Dong, M.; Yang, Z.; et al. Antimicrobial Properties of Chitosan-Functionalized Nanofibers. *Int. J. Biol. Macromol.* **2016**, *89*, 484–488.
25. Rajan, M.; Kumar, P.; et al. Synthesis and Characterization of Biocompatible Nanocomposites for Wound Healing Applications. *RSC Adv.* **2017**, *7*, 46271–46285.
26. Paduraru, A.; Ghitulica, C.; Trusca, R.; et al. Development of Advanced Materials for Wound Healing: A Comprehensive Review. *Materials* **2019**, *12*, 1859.
27. Houreld, N. N.; Abrahamse, H. The Role of Light Therapy in Treating Diabetic Foot Ulcers. *Diabetes Technol. Ther.* **2010**, *12*, 971–978.
28. Ayuk, S. M.; Houreld, N. N.; Abrahamse, H. Photobiomodulation Therapy for Diabetic Wound Healing. *Diabetes Technol. Ther.* **2012**, *14*, 1110–1117.
29. Barud, H. G.; Silveira, L. M.; et al. Biocompatible Materials for Bone and Wound Healing Applications. *Carbohydr. Polym.* **2015**, *128*, 41–51.
30. Evans, D. H.; Abrahamse, H. Photodynamic Therapy for Cancer: A Focus on Wound Healing. *Photoimmunology Photomed.* **2008**, *24*, 199–210.
31. Hosseini, E.; Sharif, A.; et al. Chemical Structure, Composition, Bioactive Compounds, and Pattern Recognition Techniques in Figs (Ficus Carica L.) Quality and Authenticity: An Updated Review. *J. Food Compos. Anal.* **2024**, *137*, 106863. https://doi.org/10.1016/j.jfca.2024.106863.
32. Dănescu, L. P.; Telipan, G.; Stoian, F. D.; et al. Review of the Use of Functional Foods in Disease Prevention. *Intech Open* **2022**, *12*, 2108–2116. https://doi.org/10.5772/65556.
33. Zhang, Y.; Li, H.; Wang, X.; Chen, Z. Fe_3O_4-Incorporated PVA-Based Fibers for Enhanced Adsorption and Catalytic Applications. *J. Mater. Sci.* **2023**, *58* (7), 1234–1245. https://doi.org/10.1007/s10853-023-07890-9.
34. Kim, J.; Park, S.; Lee, D. Nanostructured Polymer-Iron Oxide Hybrid Materials with Tunable Mesoporosity. *Adv. Funct. Mater.* **2022**, *32* (14), 2200014. https://doi.org/10.1002/adfm.202200014.
35. Hawkins, D. H.; Abrahamse, H. The Role of Photobiomodulation in Diabetic Wound Healing. *Lasers Surg. Med.* **2006**, *38*, 74–83. https://doi.org/10.1002/lsm.20235.

Figures

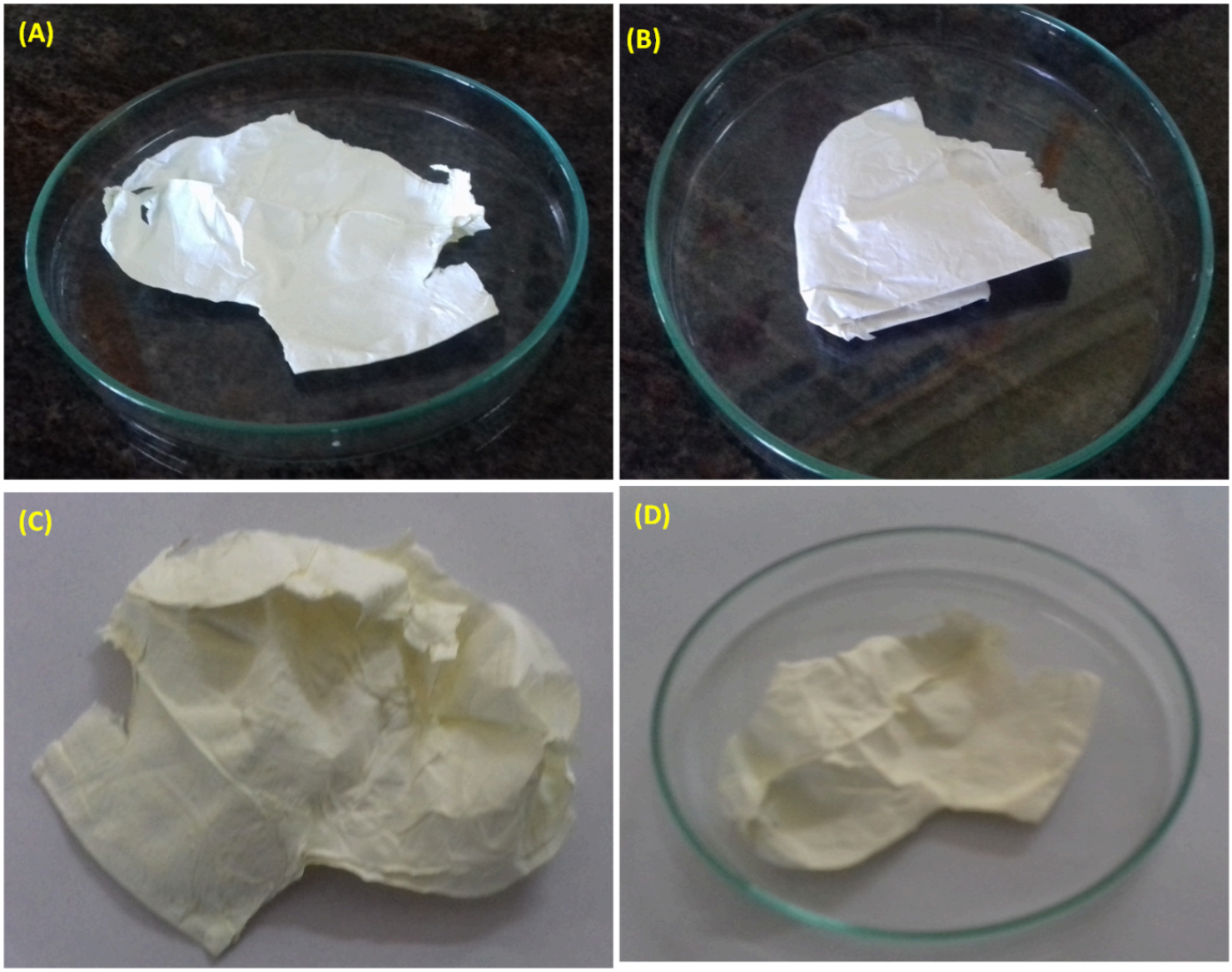

Figure 1

Prepared fibrous composites from the electrospinning method. (A) PVA, (B) Pec-30%PVA (C) Pec-30%PVA/Fe_3O_4 and (D) Pec-30%PVA/2%Fe_3O_4/FC extract composites.

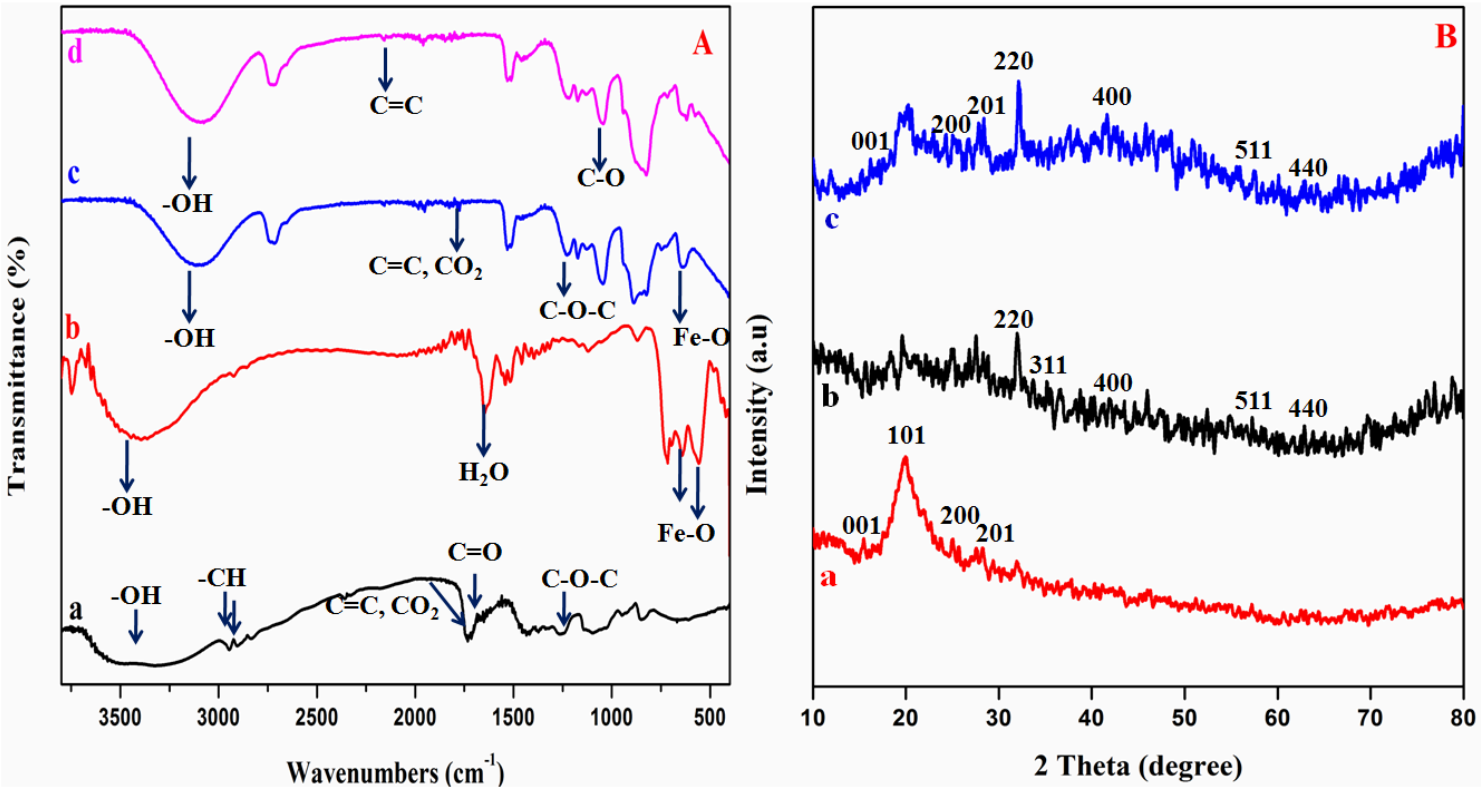

Figure 2

A) FT-IR spectrum of a) Pec-PVA, b) Fe_3O_4, c) Pec-PVA/Fe_3O_4, and d) Pec-PVA/Fe_3O_4/FC; and B) XRD patterns of a) Pec-PVA, b) Pec-PVA/Fe_3O_4, and c) Pec-PVA/Fe_3O_4/FC composites.

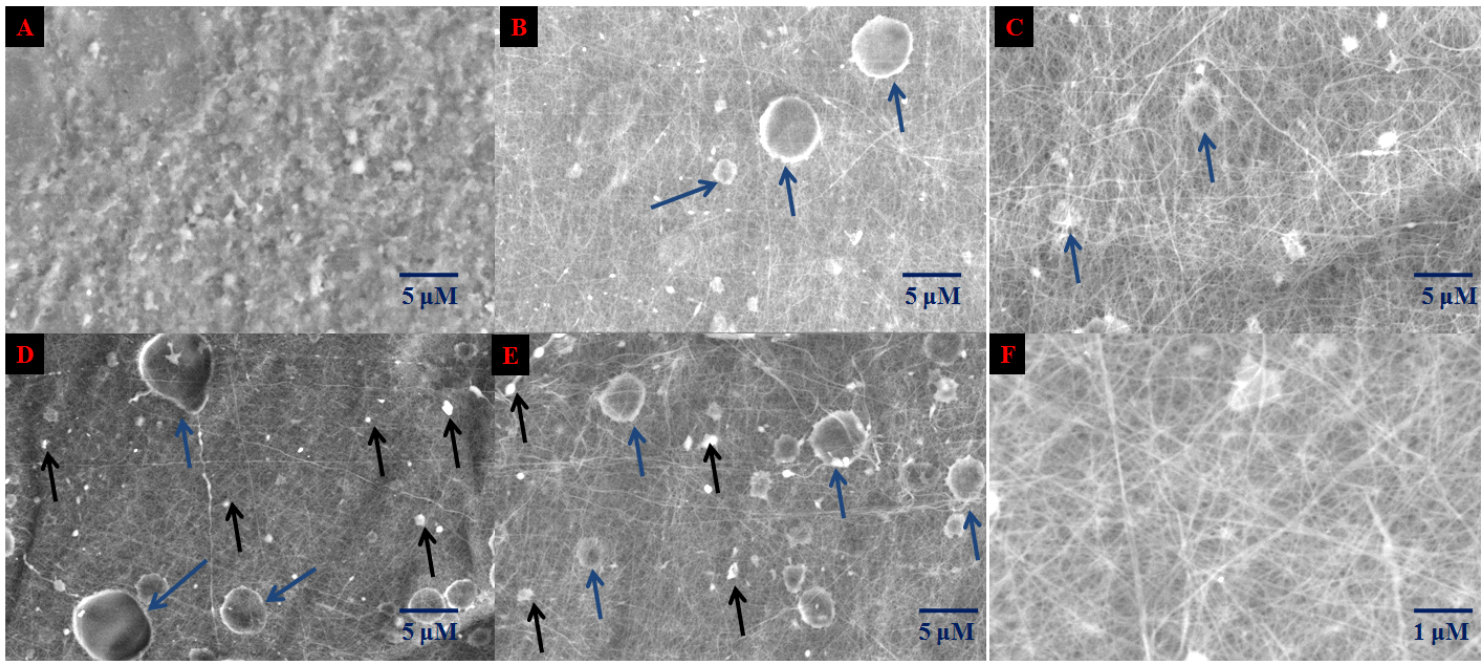

Figure 3

SEM morphology of A) pectin solution, B) Pec-10% PVA, C) Pec/ 30% PVA, D) Pec/ 30% PVA/ 20% Fe_3O_4, E) Pec/ 30% PVA/ 2% Fe_3O_4 and F) Pec/ 30% PVA/ 2% Fe_3O_4/ FC extract. Blue arrows indicate the presence of pectin particles and black arrows indicate the presence of MNPs in the fibrous networks.

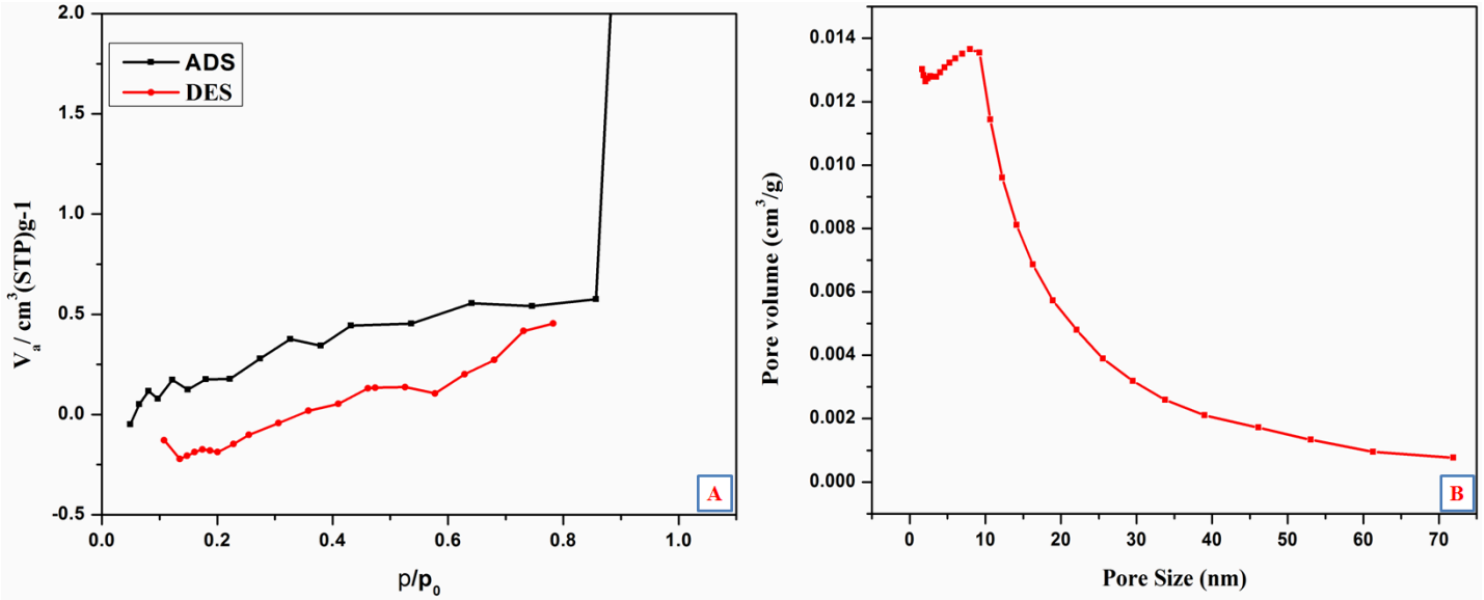

Figure 4

(A) N_2 adsorption and desorption isotherms at 77 K and (B) pore size distribution of Pec/ PVA/ Fe_3O_4/ FC fiber.

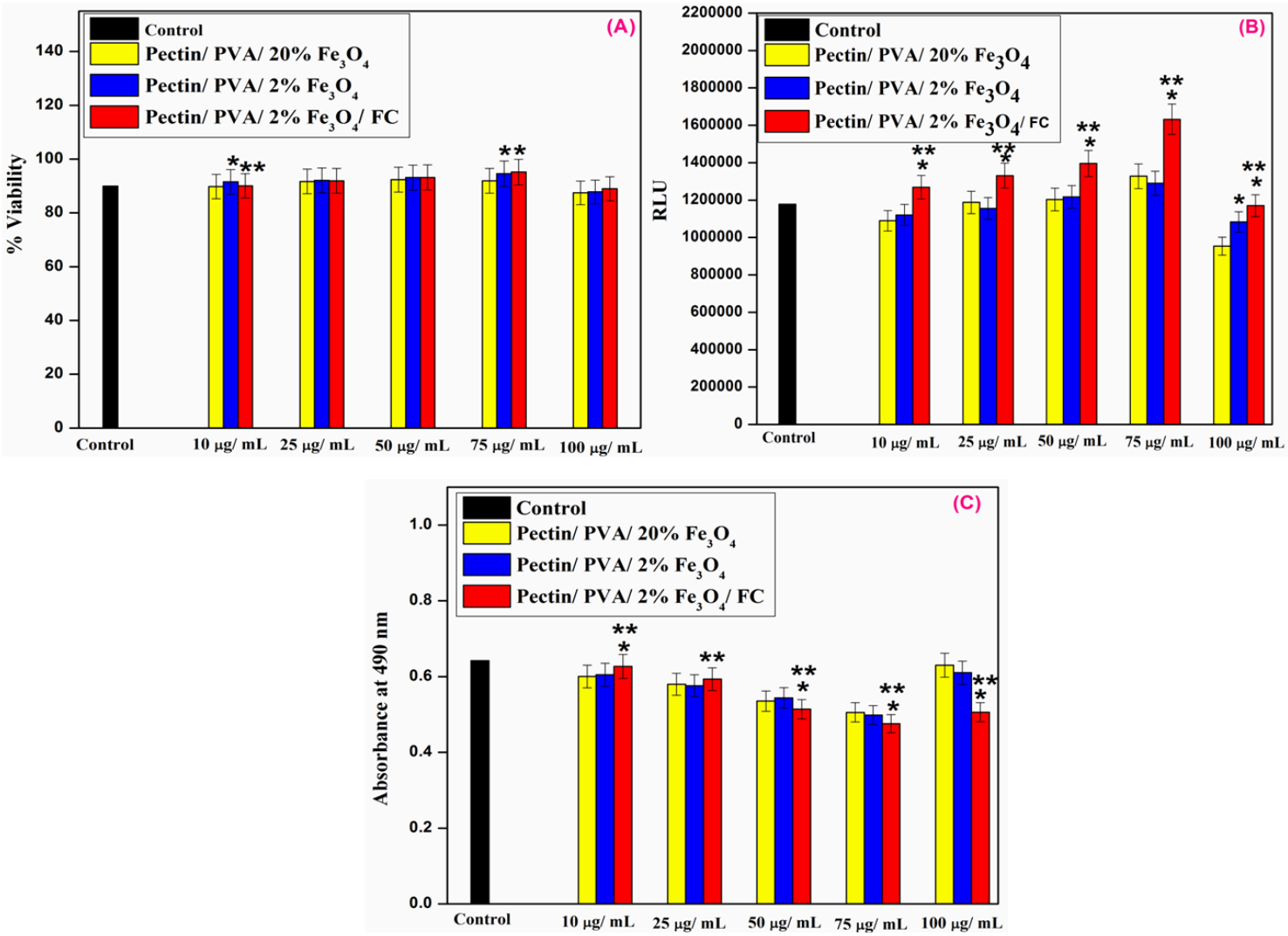

Figure 5

Cell viability of fibrous composites composed of Pectin-PVA/20% Fe_3O_4, Pectin-PVA/2% Fe_3O_4, and Pectin-PVA/2% Fe_3O_4/FC /FC at various concentrations using the following methods: (A) Trypan Blue Exclusion Assay, (B) ATP Luminescence Assay, and (C) LDH Cytotoxicity Assay. Data are presented as mean ± SEM (n = 3). Statistical significance is indicated as *P ≤ 0.05 compared to Pectin-PVA/20% Fe_3O_4 at the same concentration, and **P ≤ 0.05 compared to the control group.*

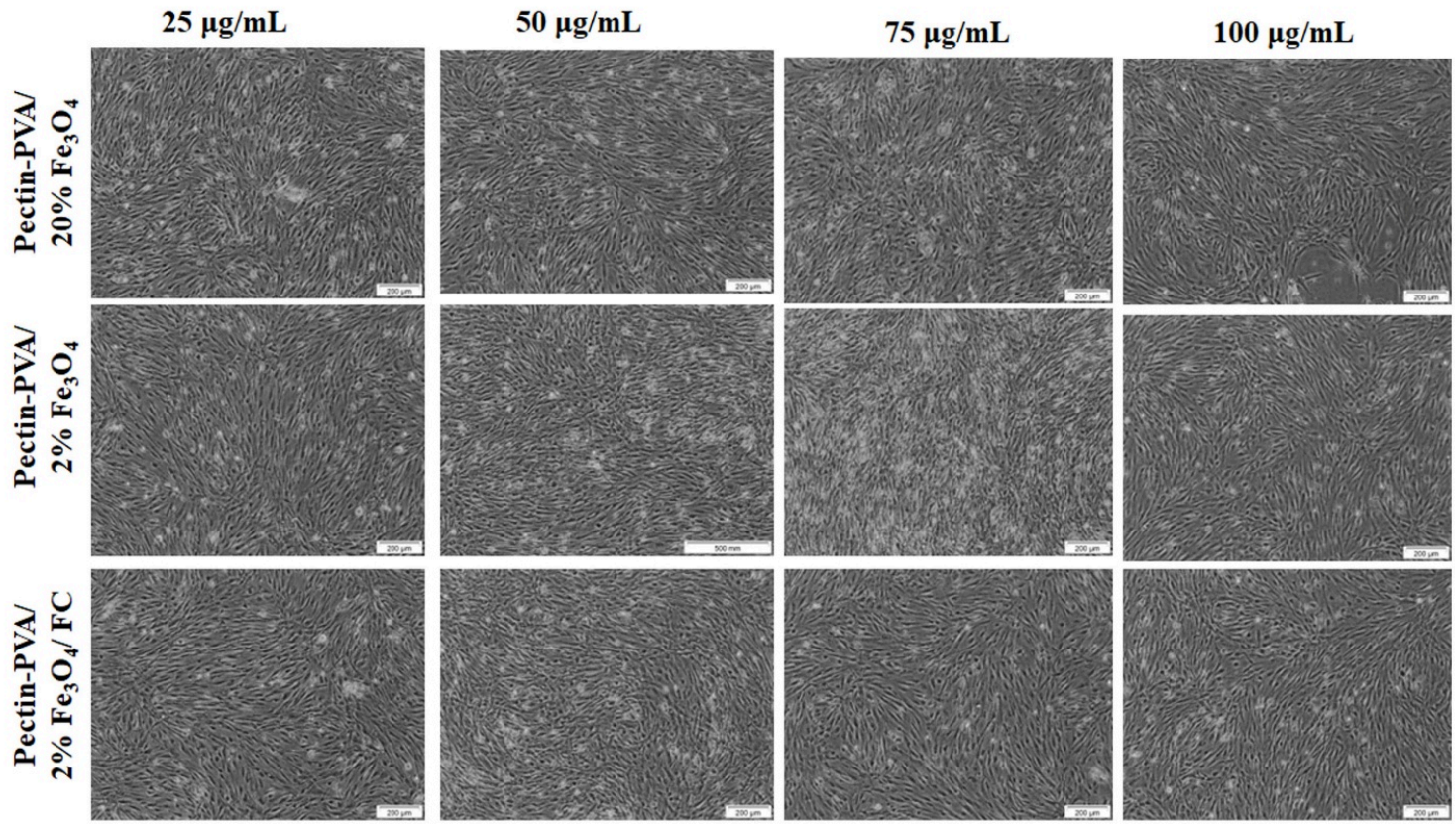

Figure 6

Optical morphology images of diabetic cell growth on different composites at different concentrations for 48 h. Magnification = ×100.

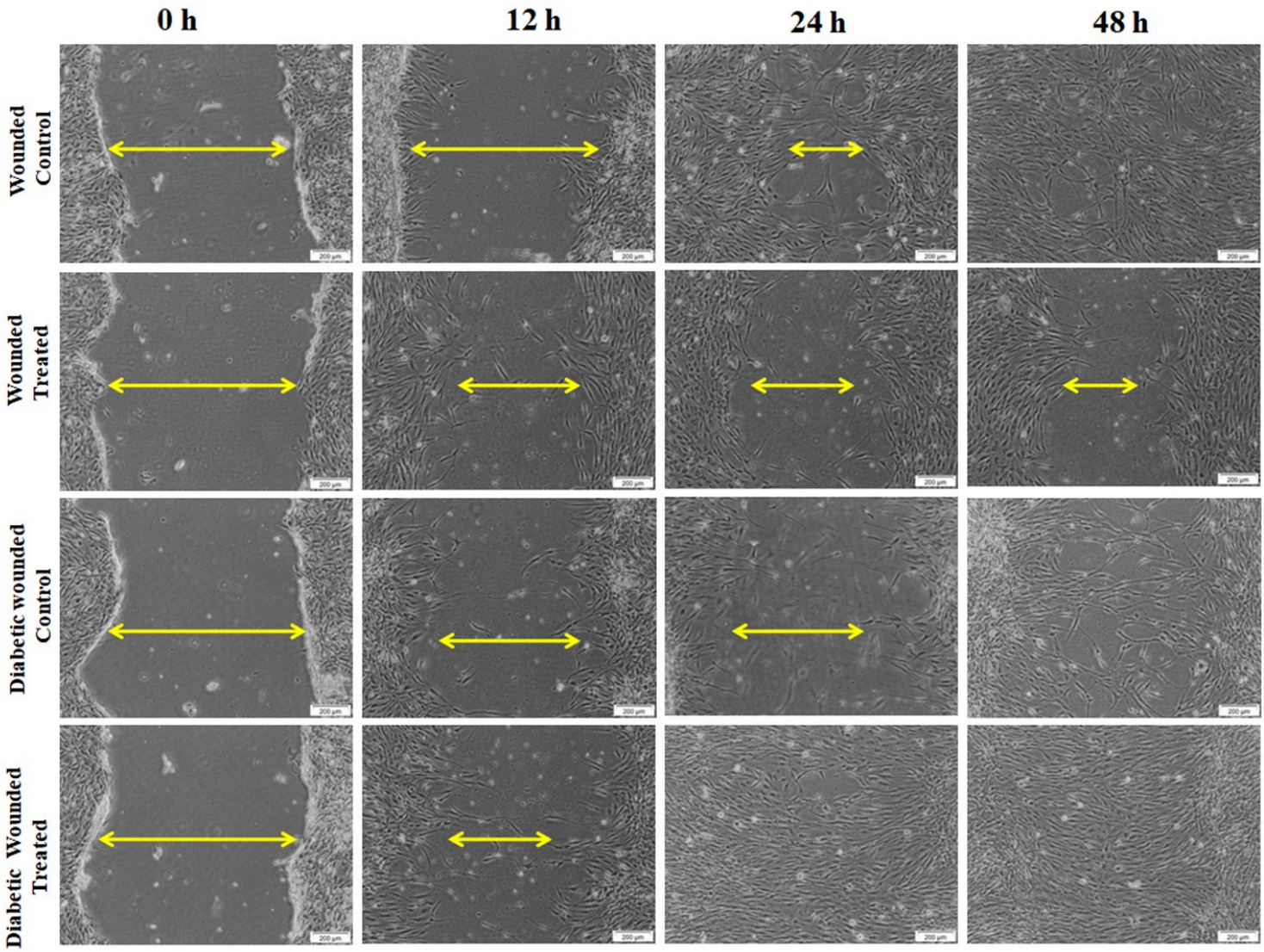

Figure 7

Optical morphology images of wounded and diabetic wounded cells. Control cells were not treated with composite, while experimental models were treated with 75 µg/mL Pectin-PVA/ 2% Fe_3O_4/ FC fibrous composite for 0, 12, 24, and 48 h. The yellow arrow indicates the central scratch ('wound') between the two wound margins.

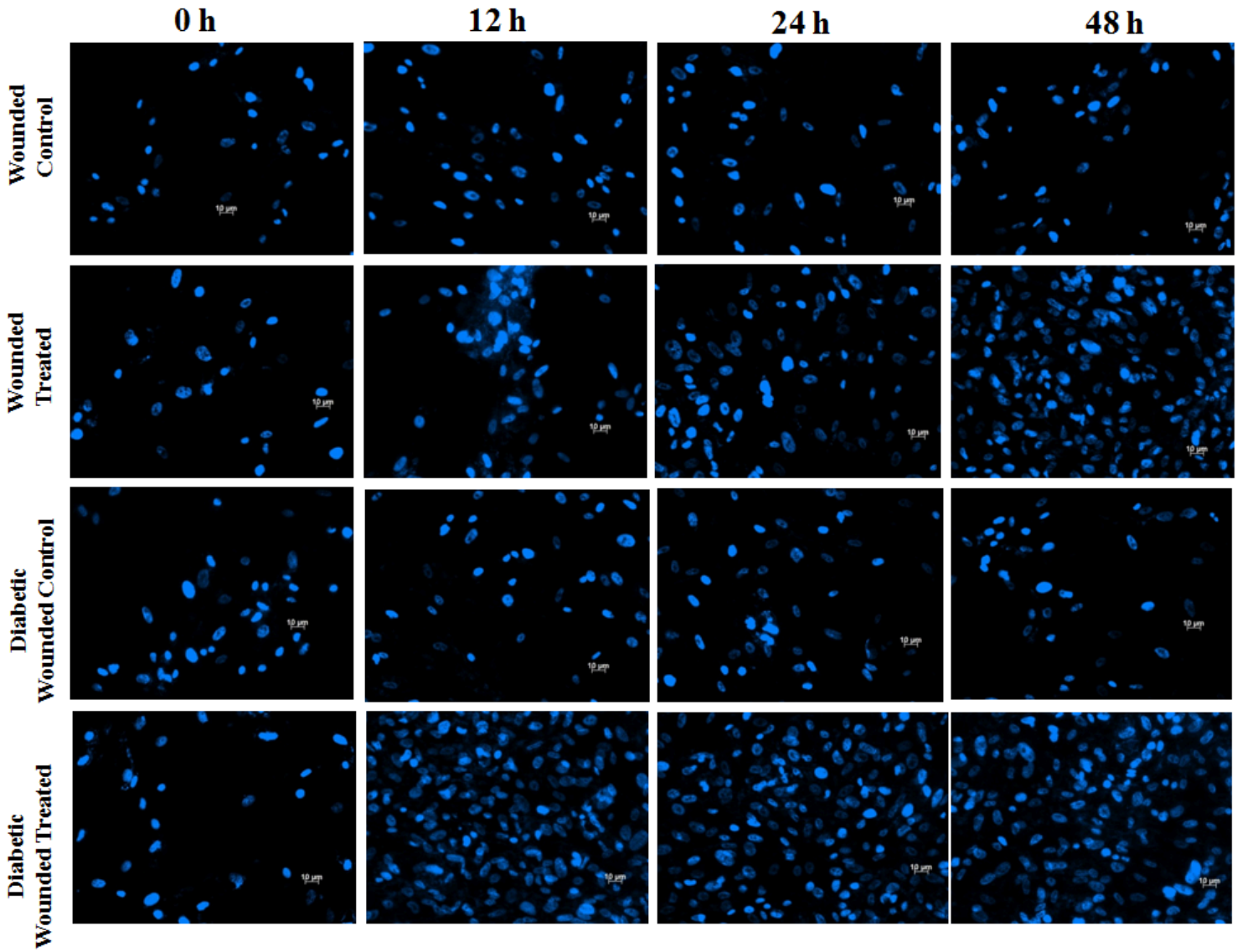

Figure 8

Nuclear morphology was determined by staining with Hoechst 33258 in wounded and diabetic wounded cells before treatment (control) and after treatment with Pectin-PVA/ 2% Fe_3O_4/ FC fibrous composite at 0, 12, 24, and 48 h. Magnification= x 200.

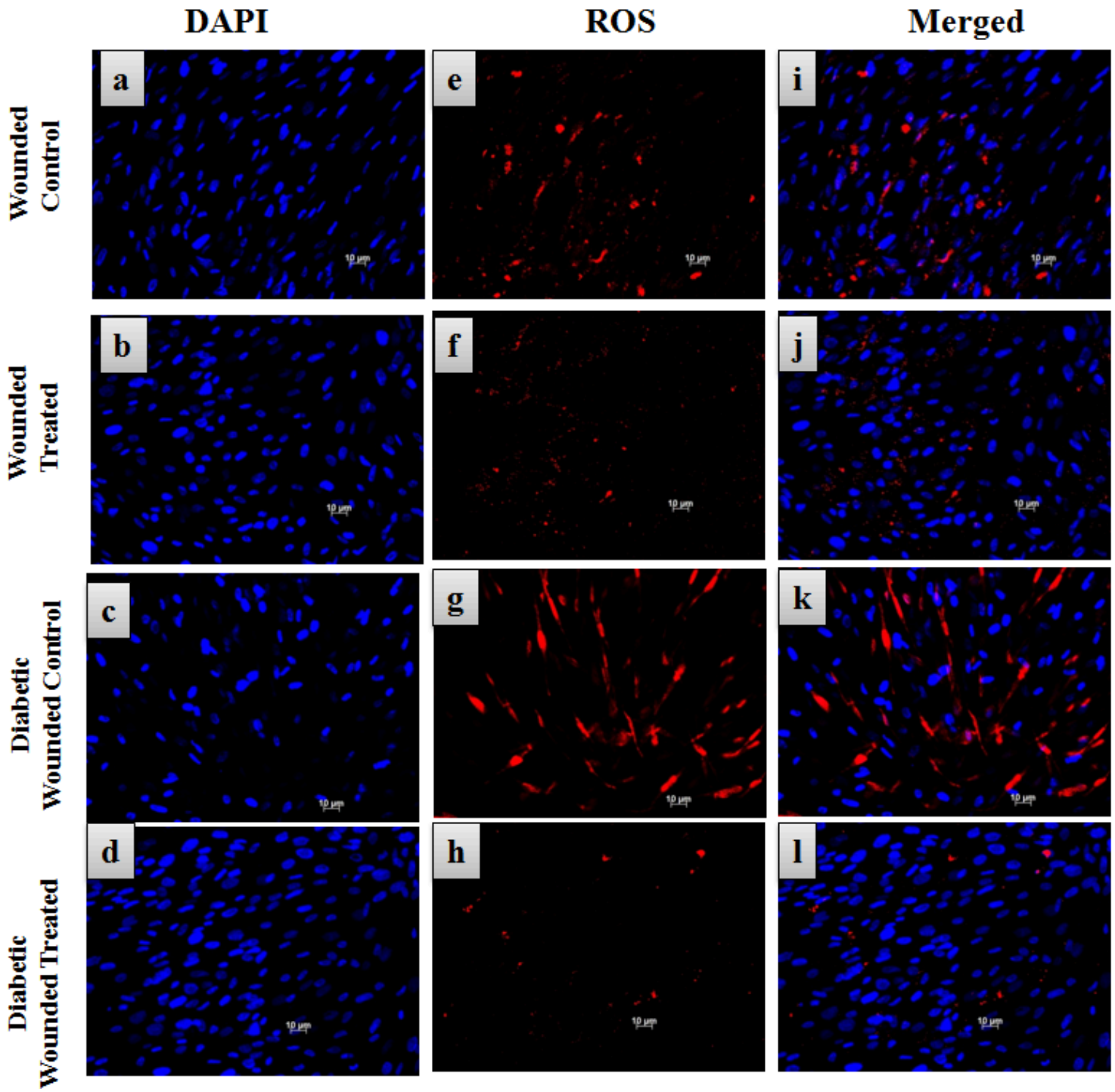

Figure 9

DAPI-stained nuclei (a-d), ROS staining (e-h), and merged images of DAPI and ROS staining (i-l) of wounded and diabetic wounded cells were observed before treatment (control) and after 48 hours of treatment with the Pectin-PVA/2% Fe_3O_4/FC fibrous composite. Images were captured at a magnification of ×200.

Supplementary Files

This is a list of supplementary files associated with this preprint. Click to download.

- GA.tif
- SupplementaryFile.doc